韓國海洋工學會誌 第13卷 第1號, pp.39~50, 1999. 2

◉ 論 文

A Shape Function for the Mesh-Free Method Using Singular Weighting Function and Three-Dimensional Applications

Yong Yun Nam*

(99년 1월 6일 접수)

특이 가중함수를 사용한 무요소법의 형상함수와 3차원 적용

남 용 윤*

Key Words : Mesh-Free(무요소), Singular Weighting(특이가중함수), Interpolant(삽간함수)

Abstract

특이 가중함수로 표현된 Shepard interpolant와 일관조건을 사용하여 무요소법 형상함수를 도출하였다. 따라서 통상의 EFGM(Element Free Galerkin Method)과는 달리 변위로 주어지는 경계조건을 자연스럽게 부과할 수 있다.

수치계산 예로서 외팔보 문제를 다루었는데 보이론과 비교하여 매우 잘 맞는 결과를 보여주고, 유한요소법과의 결합도 자연스럽게 이루어짐을 보인다. 또 penny-shaped 균열을 다루는데, 응력확대계수는 균열 표면의 변위로부터 직접 계산하여 해석해와 비교한다.

1. Introduction

The elegance of the finite element method gives it considerable appeal, for example, from the standpoint of simplicity, local approach, variational foundation, robustness, etc., as a powerful tools. However, one of its drawbacks is the difficulty of meshing complicated bodies. This requires new methodology for relaxing the strict requirement on the element definition of FEM

Recently, promising methods, which are refered to as mesh-free methods, have been reported. Mesh-free methods have some advantages over FEM. Of these, the dominant superiority is that mesh-free methods, as the name implies, do not require defined elements. Because of this, they have great potential especially in the computational fracture mechanics because it is not an easy task for both analysts and programmers to mesh cracked bodies. This work was actually motivated by the need for the auto-modelling of cracked bodies.

* 종신회원, 한국기계연구원 구조시스템연구부

Mesh-free methods have been formulated with shape functions from different sources, for example, Smooth Particle Hydrodynamic (SPH), Moving Least-Squares Method(MLS), Partition Unity Method(PUM). But they can be unified in PUM, in fact, SPH and MLS are special cases of PUM. These formulations have been well reviewed in detail by Belytschko *et al.*[1].

Initially, mesh-free method appeared in conjunction with SPH. Independently Nayroles[2] developed the diffuse element method(a type of mesh-free method) using least square fitting and Galerkin formulation. Later, Belytschko *et al*[3] improved it further and found that the diffuse element method is connected to the moving least-squares method which was developed to fit large scattered data, as reported, for example, by Lancaster and Salkauskas[4]. Belytschko *et al*[3] were the first to use the name "Element Free Galerkin Method(EFGM)"(hereafter MFGM is uesd rather than EFGM). PUM appeared some time ago, and has received considerable attention recently, Franke and Nielson[5] Renka[6], Babuska *et al.*[7].

Since the studies by Nayroles[2] and Belytschko[3] appeared, many publications on MFGM and its applications have been reported, see Lu *et al.*[8] for new implementation, Belytschko *et al.*[9] for coupling with the finite element method, Krysl and Belytschko[10] for thin plate analysis, Belytschko *et al.*[11] for dynamic fracture problems, Fleming *et al.*[12] for enriching the crack tip displacement field on MFGM. Krysl *et al.*[13] discussed convergence of shape function. Belytschko *et al.*[14] applied MFGM to three-dimensional fluid problem. Additional studies and applications are required, however, to make MFGM as robust a tool as FEM.

Most MFGM studies above are based on MLS in conjunction with nonsingular weight function. The shape function from MLS with nonsingular weight function does not constitute true interpolation because it does not pass through the data points exactly. The non-interpolation nature of shape function causes difficulties in imposing essential boundary conditions. To remedy the problem, Belytschko relied on a Lagrange multiplier[3] and coupling with FEM[9] However, these did not appear to be entirely satisfactory in terms of computation and formulation respectively. However coupling with FEM can be a very useful trick for improving computational efficiency.

On the other hand Lancaster and Salkauskas[4] showed in surface fitting that a singular weight function gives an interpolation nature to MLS. Using this approach, Kaljevic and Saigal[15] formulated MFGM with no difficulty to impose essential boundary conditions.

In this paper a shape function having an interpolation nature is carved from a Shepard interpolant and consistency condition. The Shepard interpolant of a singular weighting function can not be used as the shape function for the problems which require C^1 or more. Hence, the present shape function is modified via consistency condition. The resulting shape function appears identical to that of MLS, when MLS employs the Shepard interpolant as the weight function. Kaljevic and Saigal[15] derived another descriptions to treat singularity which aries when integration points coincide with data points. The present shape function removes the singularity without additional algebraic manipulations.

On the other hand, three-dimensional applications of MFGM is less frequent than two dimensional cases. The present shape function is applied to three-dimensional problems. One example for curve fitting, two examples for cantilever bending are provided in this paper. One example of cantilever bending shows that coupling with FEM can be made naturally without additional efforts. Finally, a penny-shaped crack immersed in a cube is solved using coupled modelling of MFGM and FEM. The

mode I stress intensity factors are evaluated directly from crack surface displacements and compared with analytical values.

2. Short Review for MFGM Formulation of MLS

Let a domain Ω, a set of data points in the domain $S=\{p^i \mid i\in\lambda\}$ where λ is a set of integers. And a function $u(x)$ are known at S. An approximation $u^c(x)$ is used to approximate $u(x)$ at arbitrary points of Ω. Here a bold x indicates a space variable, the components of which are denoted by (x,y,z). Through this paper "m" is used to indicate the dimension of a base, "n" the number of data points considered and superscripts data points unless special comments.

Let the approximation be:

$$u^c(x)=q^T(x)c(x) \tag{1}$$

where q is a complete base and $c(x)$ a one column coefficient matrix for the base.

The coefficient $c(x)$ can be obtained by minimizing a weighted norm:

$$I=\sum_{i=0}^{n} w(x,x^i)[u^i-q^T c(x)]^2 \tag{2}$$

where $w(x,x^i)$ is a weighting function. After some algebraic manipulations $c(x)$ can be expressed Eq.(3).

$$c(x)=A^{-1}BU \tag{3}$$

where the matrix A, B and U are defined by

$$A=\sum_{i=1}^{n} w^i(x)Q^i \tag{4}$$

$$w^i(x)=w(x,x^i)$$

$$Q=[q(x^i)q^T(x^i)]: m\times m \text{ matrix}$$

$$B=[w^1 q(x^1),\cdots,w^n q(x^i)]: m\times n \tag{5}$$

$U=[u(x^i)]$: one column matrix of n elements.

The shape function is derived by combining $c(x)$ and the base as bellow.

$$\phi(x)=q^T A^{-1}B \tag{6}$$

The weight function should be differentiable as many time as required. The exponential function is frequently used.

$$w^i(d^{i2k})=\frac{e^{-(d^i/c)^{2k}}-e^{-(d_{mi}/c)^{2k}}}{1-e^{-(d_{mi}/c)^{2k}}},\ d^i\le d_{mi} \tag{7}$$

$$w^i(d^{i2k})=0,\ d^i>d_{mi}$$

where d^i is the distance from x to x^i, d_{mi} the radius of influence domain, k an integer and c (the denominator of d^i and d_{mi}) a constant controlling the relative weight.

3. A New Shape Function

Using the shape function Eq.(6) to impose essential boundary conditions is a problem because it is not a true interpolation. Belytschko[3] has proposed the use of Lagrange multiplier to remedy the problem as is shown below.

$$\int_\Omega \delta(\nabla_s v^T)\sigma d\Omega-\int_\Omega \delta v^T b d\Omega-\int_{\Gamma_t}\delta v^T \bar{t}d\Gamma$$

$$-\int_{\Gamma_t}\delta\lambda^T(u-\bar{u})d\Gamma-\int_{\Gamma_t}\delta v^T\lambda d\Gamma=0\ ,$$

$$\forall\delta v\in C^1,\ \delta\lambda\in C^0 \tag{8}$$

where v is a test function and λ Lagrange multiplier.

The above strategy will bring about additional degrees of freedom at the nodes which are associated with essential boundary conditions.

It is noteworthy that the Shepard interpolant of singular weighting function is an interpolation which passes through data points, but which has C^0 continuity. The first derivatives vanish at the

data points. However, we are to start the formulation with the Shepard interpolant. Let the shape function be:

$$\phi(x) = s(x)^T \tag{9}$$

where $s(x)$ is Shepard interpolant(one column matrix of n elements), whose components are obtained from singular weighting function $w^i(x)$ as shown below.

$$s^i(x) = \frac{w^i(x)}{\sum_{j=1}^{n} w^j(x)} . \tag{10}$$

which implies

$$\sum_{i=1}^{n} s^i(x) = 1. \tag{11}$$

Eq.(9) is not suitable for the problems requiring C^1 continuity or more like FEM, and, thus a modification is given to it.

$$\phi(x) = c^T(x)\bar{s}(x) \tag{12}$$

where $c(x)$ is the coefficient matrix(one column matrix of n elements) and $\bar{s}(x)$ the diagonal matrix($n \times n$) whose elements are the same as $s(x)$. Again $c^T(x)$ is described as

$$c^T(x) = a^T(x) q_I \tag{13}$$

where $a(x)$ is the coefficient matrix(one column matrix of m elements) and q_I is the ($m \times n$) matrix whose columns are the value of base at each data point.

The convergency of solution in FEM is an important property. The linear consistency condition and stability guarantee the convergence. Here the consistency condition can be the constraint to determine $a(x)$. The linear consistency is satisfied automatically, if the next reproducibility is fulfilled.

$$\phi(x) q_I^T = q^T(x) \tag{14}$$

$$a^T(x) q_I \bar{s}(x) q_I^T = q^T(x) \tag{15}$$

After some algebraic manipulations, Eq.(15) is recasted into

$$A a(x) = q(x) \tag{16}$$

where $A = q_I \bar{s}(x) q_I^T$, which is equivalent to next expression.

$$A = \sum_{i=1}^{n} s^i(x) q(x^i) q^T(x^i) \tag{17}$$

If A is invertible, the unknown coefficient $a(x)$ is obtained as below.

$$a(x) = A^{-1} q(x) \tag{18}$$

Consequently the shape function is described as

$$\phi(x) = q^T(x) A^{-T} q_I \bar{s}(x) . \tag{19}$$

Here it is easy to confirm that $\phi(x_i) = 1$ which indicates that Eq.(19) is a true interpolation.

There are no singularities in Eq.(17) and Eq.(19) because of $\lim_{x \to x^i} s^j(x) = \delta_{ij}$, so no additional description is needed to remove them. If we do the matrix multiplications for $q_I \bar{s}(x)$ of Eq.(19), it becomes matrix B of Eq.(5). Thus, the present shape function is identical to that of MLS. In order to save the matrix operations reserved in Eq.(19), it is desirable to carry this out in the order from left to right(we have not to build matrix B explicitly as Eq.(6)).

4. Base And Weighting Function

4.1 The base

A weak point of MFGM is that the matrix A frequently becomes a poorly conditioned matrix.

Actually poor conditioning degrades the accuracy of solution seriously, and, in some cases, it is impossible to obtain solutions. The use of a linear base rectifies this problem.

On the other hand, the Shepard interpolant is not suitable for MFGM since it has C^0 continuity as mentioned previously. To improve this, the Shepard interpolant is modified by Eq.(19). If a singular weight function is used, the linear base is insufficient for the modification. A quadratic base is minimally required. This can be easily explained with Eq.(19). The Shepard interpolant has plateaus at the data points. The modifier which precedes the Shepard interpolant causes a flattening and heeling of the plateaus. Here the linear base can not provide a sufficient cure because the plateaus develop with the rate of inverse of the distance.

Two approaches have been discussed to suppress the effect of poor conditioning[12]; using an orthogonal base and less multiplying operations for inverting matrix $\boldsymbol{A}$, for instance, $\boldsymbol{LDL}^T$ decomposition. But these two methods seem not to work very well. Actually Gramm-Schmidt orthogonalization with a quadratic base was tested prior to this study, but returned poor solutions.

Numerous studies are required in finding a good base. But it appears that poor conditioning is, to some extent, inherent in the pattern of node distribution. In this context it would be desirable to share our efforts in finding how to generate nodes properly.

In this study, a quadratic base as below is used.

$$[1, \zeta, \eta, \xi, \zeta\eta, \eta\xi, \xi\zeta, \zeta\eta\xi, \zeta^2, \eta^2, \xi^2] \qquad (20)$$

where,

$$\zeta = x - x_0 \ , \quad \eta = y - y_0 \ , \quad \xi = z - z_0$$

$$x_0 = \sum_{i=1}^{n} s^i(\boldsymbol{x}) x^i \ , \quad y_0 = \sum_{i=1}^{n} s^i(\boldsymbol{x}) y^i \ ,$$

$$z_0 = \sum_{i=1}^{n} s^i(\boldsymbol{x}) z^i$$

The new origin $\boldsymbol{x}_0$ is the weighted average of coordinates of nodes contained in the influence domain. By that the constant element of base is orthogonal to linear elements. For convenience it is still necessary to use $\boldsymbol{x}$ instead of ζ, η, ξ.

To reduce the dimension of matrix $\boldsymbol{A}$, the Gramm-Schmidt orthogonalization is applied only to quadratic bases, generating new base as below.

$$q_i(\boldsymbol{x}, \cdot) = p_i(\cdot) - \sum_{j=1}^{n} s^j(\boldsymbol{x}) p_i(\boldsymbol{x}^j), i = 5, 11 \qquad (22)$$

Such transformation calls for additional computations in the derivation of Eq.(19), because of the base should be derived even at data points due to the Shepard interpolant(see Eq.(22)). But the second term of Eq.(22) is to be dropped in present derivation. Later it will be seen in the numerical examples that this is a good approximation. Hence the derivatives of base and shape function are described as

$$q_i'(\boldsymbol{x}, \cdot) = p_i' \qquad (23\text{-}1)$$

$$\phi'(\boldsymbol{x}) = [\boldsymbol{q}^T(\boldsymbol{x}) \boldsymbol{A}^{-T} + \boldsymbol{q}^T(\boldsymbol{x})(\boldsymbol{A}^{-T})'] \boldsymbol{q}_I \bar{s}(\boldsymbol{x}) + \boldsymbol{q}^T(\boldsymbol{x}) \boldsymbol{A}^{-T} \overline{\boldsymbol{q}_I \bar{s}'}(\boldsymbol{x}). \qquad (23\text{-}2)$$

Here by taking into account the orthogonality between the constant element of base and other elements, Eq.(23-2) is expressed as

$$\phi'(\boldsymbol{x}) = [\boldsymbol{q}^T(\boldsymbol{x}) \boldsymbol{A}^{-T} + \boldsymbol{q}^T(\boldsymbol{x})(\boldsymbol{A}^{-T})'] \boldsymbol{q}_I \bar{s}(\boldsymbol{x}) [I + \boldsymbol{q}^T(\boldsymbol{x}) \boldsymbol{A}^{-T} \overline{\boldsymbol{q}_I}] \bar{s}'(\boldsymbol{x}) \ . \qquad (23\text{-}3)$$

Of course matrix $\boldsymbol{A}$, $\boldsymbol{q}(\boldsymbol{x})$, and $\boldsymbol{q}_I$ have smaller dimensions than before by one.

4.2 Weighting function

The singular weight presented by Lancaster and Salkauskas[4] is used in the numerical calculations.

$$w^i(d^i)=\frac{\rho^2}{(d^i)^2}(1-\frac{d^i}{\rho})^2\ ,\quad d^i\le\rho$$
$$w^i(d^i)=0,\qquad d^i>\rho \tag{24}$$

where d^i is the distance between $\boldsymbol{x}$ and $\boldsymbol{x}^i$, and ρ is the radius of the influence domain. The first derivative of weighting function is written by

$$w^i_{,x_j}=\frac{2\rho^2(x_j-x_j^i)}{(d^i)^4}(\frac{d^i}{\rho}-1). \tag{25}$$

5. Numerical Examples

5.1 Curve fitting

To inspect the behavior of the present shape function, a curve fitting is supplied here. The curve is shaped by 4 data points equally spaced; (-2,0), (-1,2), (1,2), (2,0). The radius of the influence domain ρ is 5. Three types of bases, $[1],[1,x]$ and $[1,x,x^2]$ are tested.

The curved is directly fitted by the shape function as below.

$$y(x)=[\phi^i(x)][u_i] \tag{26}$$

Fig.1 shows the results. As expected the fitting passes through the data points. The constant base denoted by $n=1$ products plateaus at data points, and the linear base seems not to improve the situation significantly. However, with the quadratic base, the curve is fitted reasonably. Fig.2 reflects its derivatives by which we well understand the need for a quadratic base. The base, $[1,x^2]$ is also tested and gives the same results as the quadratic base. Kaljevic and Saiga[15] have noted that the linear base gives poor solutions in beam bending problem due to the inherent nature of the beam bending. However, the lower accuracy of a linear base in bending problems is inherent in the nature of shape function itself of singular weight function as shown in Fig.2.

Matrix $\boldsymbol{A}$ can not be inverted at data points, and the fitting becomes even more useless at its neighboring points as shown in Fig.3 which shows some unrealistic oscillations near the data point. This problem can be circumvented easily by shifting the field points very small distance from the data points only when evaluating matrix $\boldsymbol{A}$. Fig.4, obtained with small shifting($=\rho\times1.8E-4$), dictates the result by the scheme.

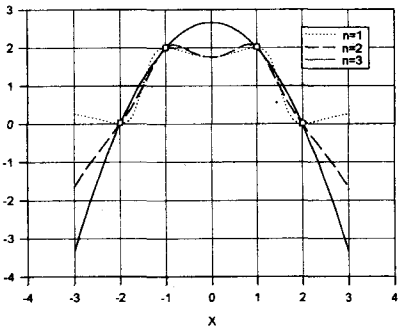

Fig. 1 Curve fitting

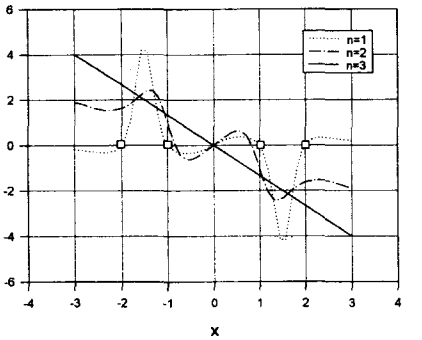

Fig. 2 Derivatives of fitted curve

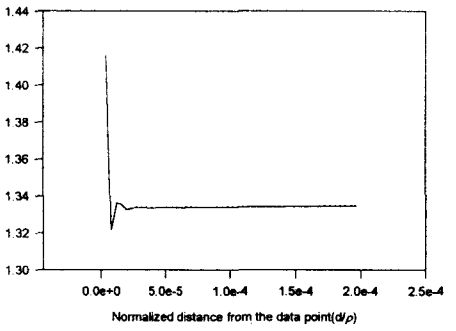

Fig. 3 Derivatives in the neighborhood of the data point $x=-1$

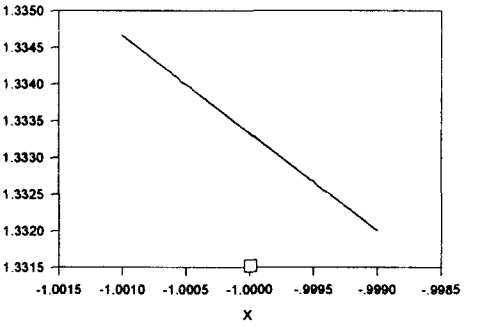

Fig. 4 Approximated derivatives in the neighborhood of the data point $x=-1$

Table 1 Patch test for 13 nodes

position of node 13	(0.1, 0.1, 0.1)					
displacement of node 13	(.30E-01, .30E-01, .90E+00)					
relative errors(%)						
integration point(x,y,z)	σ_x	σ_y	σ_z	σ_{xy}	σ_{yz}	σ_{zx}
at all point	0.00	0.00	0.00	0.00	0.00	0.00

Table 2 Patch test for 15 nodes

position of node 13			(0.2, 0.3, 0.6)					
displacement of node 13			(.5887E-1, .9066E-1, .5747E+0)					
relative errors(%)								
integration point(x,y,z)			σ_x	σ_y	σ_z	σ_{xy}	σ_{yz}	σ_{zx}
.113	.113	.113	1.11	1.05	4.55	.03	1.03	.36
.887	.113	.113	.11	.23	.47	.15	.30	.66
.500	.500	.113	1.00	1.00	3.67	.13	.06	.16
.113	.887	.113	.54	.63	.47	.35	.49	.31
.887	.887	.113	.41	.27	.47	.19	.35	.46
.500	.113	.500	.68	.55	1.45	.13	1.81	.81
.113	.500	.500	.60	.87	2.44	.13	1.32	2.92
.500	.500	.500	.57	.34	1.45	.01	.67	1.22
.113	.887	.500	.36	.48	.96	.22	.26	.06
.500	.887	.500	.03	.01	.00	.06	.01	.17
.113	.113	.887	.15	.08	2.94	.15	.43	.00
.887	.113	.887	.30	.53	.00	.04	.33	.42
.500	.500	.887	.30	.22	1.94	.13	.11	.03
.113	.887	.887	.82	.61	.47	.09	.43	.41
.887	.887	.887	.12	.05	.48	.65	.07	.16

5.2 Patch test

Present shape function is designed to satisfy consistency condition, and, hence it reproduces the constant strain state. Simple patch tests(test B[16]) are performed to determine the constant strain state.

For this purpose, a cube is selected. As material parameter Poisson's ratio is 0.3. The configuration of the cube is shown in Fig.5. To produce the constant strain state, essential boundary conditions are imposed on nodes except for Node 13.

The results were taken on Gaussian integration points(3×3×3). Table 1 and 2 show typical results; Table 1 for 13 nodes, and Table 2 for 15 nodes. The relative errors were evaluated by $((\sigma_{exact}-\sigma_i)/\sigma_{z,exact})\times 100(\%)$.

The patch test of 13 nodes(Table 1) shows the exact constant strain state, while the case of 15 nodes gives relatively less accuracy. It appears that too many nodes exceeding the base size are not desirable. The more eccentric node 13 is, the more errors it gives in the case of 15 nodes, but the case of 13 nodes gives the exact constant state regardless of the position of node 13.

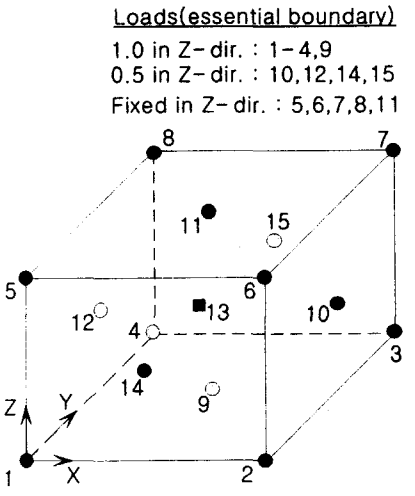

Fig. 5 The cube for patch tests

5.3 Cantilever bending

The cantilever, $L=19.6(m)$, $B=2.0(m)$, is generated as Fig.6. Dashed lines designate cell division and solid circles nodes. The radius of influence is $2.6(m)$. As an essential boundary the left end is fixed, and point forces are imposed on the nodes of the other end. Total $1,500(KN)$ is shared properly on the nodes of right end. The number of integration points is $(4\times4\times4)$ per a cell. As material parameters, Young's modulus is $200(GPa)$ and Poisson's ratio 0.3.

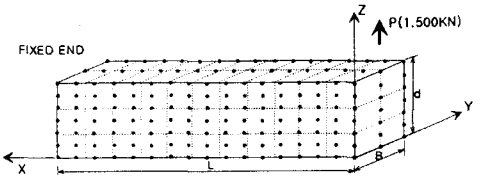

Fig. 6 Cantilever modelled by MFGM

The bending stresses are compared with beam theory in Fig. 7, and show good agreement.

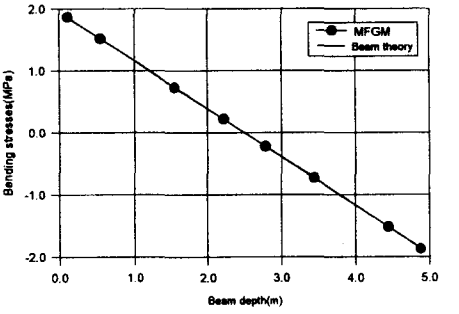

Fig. 7 Bending stresses at $x=10.81$

However, the shear stresses, as shown in Fig.8, appear to have small discrepancies which are supposed due to some numerical errors from the lack of nodes in the depth direction and the nonlinear shear stress distribution in the

direction. The deflections of the neutral axis are plotted in Fig. 9, which shows good agreement. Shear deflections are accounted in the results of beam theory.

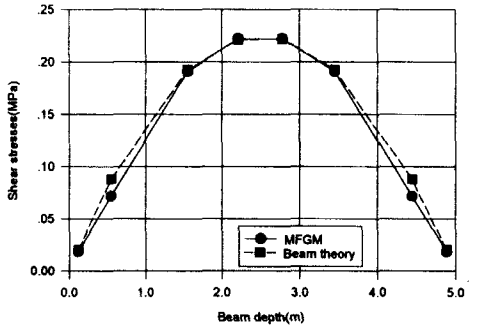

Fig. 8 Shear stresses at $x=10.81$

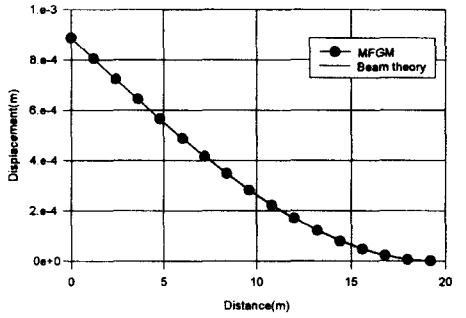

Fig. 9 Deflections of neutral axis

5.4 Coupling with FEM

There are no problem in imposing essential boundaries since the present shape function is an interpolation. Therefore we understand that the coupling is for computational efficiency and to give flexibility to MFGM. In this example, we show that coupling with FEM is made naturally. Consider the cantilever, $L=19.6(m)$, $B=2.0(m)$, $d=4.0(m)$. The lower half is meshed by FEM and upper by MFGM. For FEM modelling nonconforming 8 node solid elements are used. Of course we have no special considerations for the coupling. Influence radius, material parameter and essential boundaries are the same as in Section 5.3. As loading, concentrated forces, total amount of $900(KN)$, are applied to the nodes of the right end.

The deflections are plotted in Fig. 11. A small discrepancy on the curve can be seen. If shear correction on the beam theory is considered, we can have overlapped curves again, as in Fig.9. Fig. 12 shows good linearity of bending stresses which indicates that the present shape function is amiable to FEM. Here shear stresses are not compared due to lack of mesh division in depth.

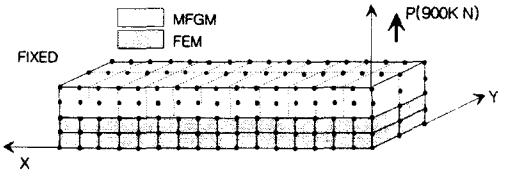

Fig. 10 Coupled modelling by MFGM and FEM

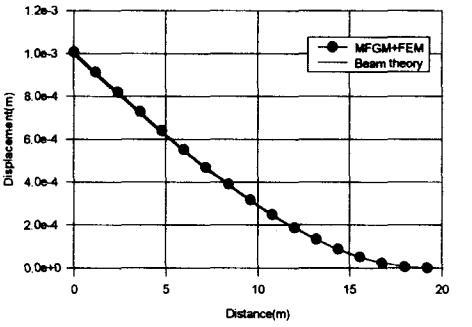

Fig. 11 Deflections of coupled modelling

5.5 Penny-shaped crack

A penny-shaped crack immersed in the right cube is considered The dimension of the cube is 100(mm) in the edge length and it is subjected to uniform tension(nominal stress is $100(MPa)$.

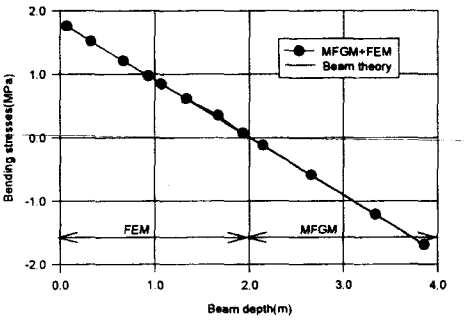

Fig. 12 Bending stresses of coupled modelling

The material parameters are 21(*GPa*) and 0.3 for Young's modulus and Poisson's ratio respectively. The penny-shaped crack, having a radius of 10(*mm*), is positioned at the center of the cube.

Taking advantage of the symmetric properties of the cube under tension, just one eighth is counted in the computation. The core of cube is meshed by cells of MFGM, and the remainder by 8-node nonconforming solid elements of FEM. The process of meshing is quite simple; first mesh the cube by FEM and delete the core for MFGM meshes(see Fig.13), next mesh the core by MFGM and generate nodes(see Fig.13), finally generate nodes along crack front(see Fig.14). Note that nodes near the crack tip appear irregular.

A (4×4×4) Gauss integration rule is used. The radius of the influence which is variable and controlled by cell size, is 1.15 times of maximum diagonal distance of each cell.

For reference, the analytical solution for an unbounded domain is used. If $a/R \leq 1/5$, the difference between numerical solutions of the finite domain and the unbounded domain is negligible. Thus the present numerical solution can be compared with the analytical stress intensity factors of penny-shaped crack in infinitive domain given below[17].

$$K_I = 2\sigma\sqrt{\frac{a}{\pi}} \tag{27}$$

The numerical stress intensity factors are evaluated directly from the crack surface displacements.

$$K_I = \frac{2G\sqrt{2\pi}}{\varkappa} \cdot \frac{\Delta V}{r} \tag{28}$$

where G is the shear modulus, $\varkappa = 3-4\nu$, ΔV the crack face displacement at a point at which the distance is r in a normal direction from crack tip.

The results are compared with the analytical solution in Fig.15. The present calculation gives uniform K_I values along the crack front except in the starting and ending regions, as well as very close to the analytical values. In fact the K_I of the present calculation are sensitive to node distributions near the crack tip. Fig.16 shows other results which are obtained from alternative node arrangement. These oscillate along the crack front. Such tendency has been shown by Belytschko[18]. These data indicate the need for additional studies relative to regulating oscillations.

6. Conclusion

The shape function for MFGM is presented in this paper The shape function is formulated by the Shepard interpolant and consistency condition instead of the MLS process. Here the Shepard interpolant is taken as partition of unity. The singular weight function is employed. in order to achieve a true interpolation.

Three-dimensional problems are solved to verify the present shape function. Simple curve fitting shows some properties of the present shape function explicitly. Two cantilever bending examples show the accuracy of present shape

function, and proves that coupling with FEM can be made without additional considerations.

Finally, a penny-shaped crack immersed in the cube is solved. Some observation are summarized as follows.

1) The resulting description of the present shape function is identical to MLS shape function, provided the Shepard interpolant as weighting is used for MLS formulation. However, the present shape function suggests that it is not advisable to preform matrix $\boldsymbol{B}$ of MLS formulation for computational efficiency.

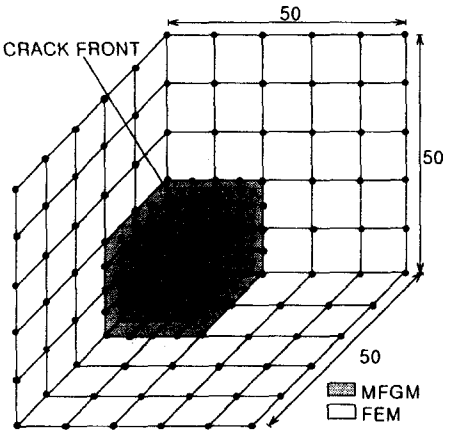

Fig. 13 Meshes of cube by MFGM and FEM

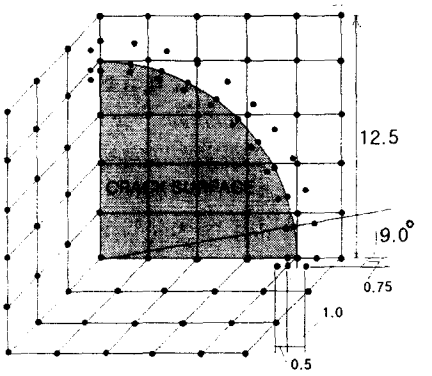

Fig. 14 Node generation along a crack front

2) The present shape function has removable singularities. Thus additional considerations are not required.

3) When using singular weight function, the use of a quadratic base, at a minimum, is inevitable for accuracy. It has been concluded that linear base gives poor solutions in beam bending problems due to the nature of the beam bending[15]. Actually the selection of the base seriously affects accuracy if a singular weight function. is used. The lower accuracy of linear base in bending problem is

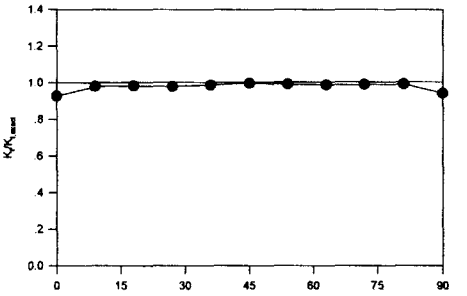

Fig. 15 Stress intensity factors

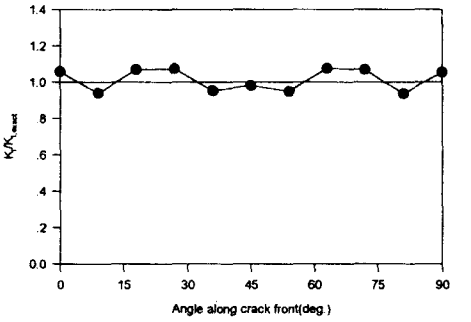

Fig. 16 Stress intensity factors of alternative node arrangement

inherent in the nature of shape function itself in the singular weighting function.

4) With a quadratic base, frequently matrix $\boldsymbol{A}$ of Eq.(17) is poorly conditioned. Two approaches[12] are not effective in improving the conditioning,

and it appears that a careful node generation can be a solution for this problem. However, such consideration has not been found in the literature.

5) K_I values of present calculation are sensitive to node distributions near the crack tip(see Fig.16). This indicates the need for additional studies related to regulating oscillations, e.g., remapping of displacements.

REFERENCES

1) T. Belytschko,Y. Krongauz, D. Organ, M. Fleming and P. Krysl, "Meshless methods:An overview and recent developments", Comput. Methods Appl. Mech. Engrg, 139, 3-47, 1996

2) B. Nayroles, G. Touzot and P. Villon, "Generalizing the finite element method: Diffuse approximation and diffuse elements", *Comput. Mech.*, **10**, 307-318, 1992

3) T. Belytschko, Y.Y. Lu and L. Gu, "Element-free Galerkin methods",*Int. J. Numer Mehods Engrg.*, Vol.37, p.229-256, 1994

4) P. Lancaster and K. Salkauskas, "Surfaces generated by moving least squares methods", *Math Comput.*, **37**, No.155, p.141-158, 1981

5) Richard Franke and Greg Nielson, "Smooth interpolation of large sets of scat-tered data", *Int. J. Numer. Methods. Engrg.*, Vol.15, p.1691-1704, 1980

6) Robert J. Renka, "Multivariate interpolation of large sets of scattered data", *ACM Trans. Math. Soft.*, 14, 2, 139-148, 1988

7) I. Babuska and J.M. Melnk, "The partition of unity method", *Int. J. Numer. Methods. Engrg.*, Vol.40, p.727-758, 1997

8) Y.Y. Lu, T. Belytschko and L. Gu, "A new implementation of the element free Galerkin method", *Comput. Methods Appl. Mech. Engrg*, 113, 397-414, 1994

9) T. Belytschko, D. Organ, Y. Krongauz, "A coupled finite element-free Galerkin method", Comput. Mech.,17, p.186-195, 1995

10) P. Krysl and T. Belytschko, "Analysis of thin plates by the element-free Galerkin method", *Comput. Mech.*,17, 26-35, 1995

11) T. Belytschko, Y.Y. Lu, L. Gu, and M. Tabbara, "Element-free Galerkin methods for static and dynamic fracture", *Int. J. Solids Structures*, 32, 17/18, 2547-2570, 1995

12) M. Fleming, Y.A. Chu, B. Moran and T. Belytschko, "Enriched element-free Galerkin methods for crack tip fields", *Int. J. Numer. methods Fluids*, 40, 1483-1504, 1997

13) P. Krysl, T. Belytschko, "Element-free Galerkin method: Convergence of the continuous and discontinuous shape functions", *Comput. Methods Appl. Mech. Engrg*, 148, 257-277, 1997

14) T. Belytschko, P. Krysl and Y. Krongauz, "A three-dimensional explicit element-free Galerkin meth-od", *Int. J. Numer. methods Fluids*, 24,1253-1270, 1997

15) Igor Kaljevic and Sunil Saigal, "An improved ele-ment free Galerkin Formulation", *Int. J. Numer. methods Fluids*, 40, 2953-2974, 1997

16) O.C. Zienkiewiccz and R.L. Taylor, "The Finite Element Method", *McGRAW-HILL*, Fourth edition, p.294, 1989

17) G.C.Sih, *Handbook of Stress Intensity Factors, Lehigh University, Bethlehem, Penn.*, 1973

18) Krysl, P. and T. Belytschko, "Application of the element free Galerkin method to the propagation of arbitrary 3D cracks", submitted to *Int. J. Numer. Methods. Engrg.*, 1997